Comments on "Synchronous Variability in the Southern Hemisphere Atmosphere, Sea Ice, and Ocean Resulting from the Annular Mode"

WARREN B. WHITE

Scripps Institution of Oceanography, University of California, San Diego, La Jolla, California

25 November 2002 and 15 October 2003

In a recent article, Hall and Visbeck (2002) stated that the southern annular mode (SAM) of Thompson and Wallace (2000) dominates all other modes of variability in the Southern Ocean. A quote from their article reads, ''However, given the overwhelming dominance of the annular mode of the real atmosphere's internal variability on all time scales greater than a few days and the favorable geometry of the SH ocean, it seems likely that when adequate observations of all ocean variability in this region exist, most of the variability will ultimately be traced not to the Antarctic circumpolar wave or ENSO, but to the SAM.'' No reference is given for the first half of this statement. Moreover, it is incorrect. Instead, the Antarctic circumpolar wave (ACW; White and Peterson 1996; Jacobs and Mitchell 1996) and the teleconnected El Niño–Southern Oscillation (ENSO) signals (Karoly 1989; Cai and Baines 2001; White et al. 2002) dominate the SAM in the real atmosphere's variability on interannual period scales.

To demonstrate this, we conduct two independent analyses on monthly mean sea level pressure (SLP) anomalies about the long-term monthly mean over the Southern Hemisphere for the 20 yr from 1982 to 2001 obtained from the National Centers for Environmental Prediction–National Center for Atmospheric Research (NCEP–NCAR) reanalysis (Kalnay et al. 1996). First, we apply complex empirical orthogonal function (CEOF) analysis (Preisendorfer and Mobley 1988) to the monthly SLP anomalies from 20° to 90°S. This methodology allows both the standing mode of the SAM (global zonal wavenumber 0) and the propagating wave of the ACW (global zonal wavenumber 2) to be revealed over the Southern Ocean within an analysis framework that allows both standing and traveling waves to be expressed. Second, we conduct the multitaper method–singular value decomposition (MTM–SVD) of Mann and Park (1999) on the same dataset for the same period. The SLP variable is the same as that used by Hall and Visbeck (2002) to characterize the SAM in their article. We apply CEOF and MTM–SVD analysis to monthly SLP anomalies that are weighted by area, following the methodology of Thompson and Wallace (2000). We did not detrend the SLP data prior to CEOF or MTM–SVD analysis. We display both the time sequence of amplitudes and the phase sequence of spatial patterns for the dominant CEOF and complex SVD modes.

The phase sequence of the leading CEOF mode of area-weighted monthly SLP anomalies explains ~28% of the total variance (Fig. 1a) and displays the global zonal wavenumber-0 pattern of the SAM. This is similar to the leading mode obtained by Thompson and Wallace (2000) from the EOF analysis of the area-weighted height anomalies of the 850-hPa pressure surface (Z_{850}), which explains 27% of the monthly Z_{850} variance from 1958 to 1997. The spatial pattern of the SAM at 0° and 90° of phase displays maximum variability along the land–sea boundary of Antarctica— in phase with weaker variability over Antarctica and out of phase with weaker variability near 45°S over the Southern Ocean. Here, the CEOF phase sequence allows for the possibility of phase propagation in the SAM. However, this CEOF mode does not exhibit any evidence of propagation because the magnitudes of weights in the pattern at 90° of phase (i.e., the imaginary component of the CEOF) are negligible compared to those in the patterns at 0° and 180° of phase (i.e., the real component of the CEOF). This verifies that the SAM is a true standing mode.

The phase sequence of the second CEOF mode of area-weighted SLP anomalies explains ~12% of the total variance (Fig. 1b) and displays the global zonal wavenumber-2 and -3 pattern of the ACW (White and Peterson 1996; Cai and Baines 2001; Venegas 2003). The ACW in the CEOF phase sequence can be seen

Corresponding author address: Dr. Warren B. White, Scripps Institution of Oceanography, University of California, San Diego, 9500 Gilman Drive, La Jolla, CA 92093-0230.
E-mail: wbwhite@ucsd.edu

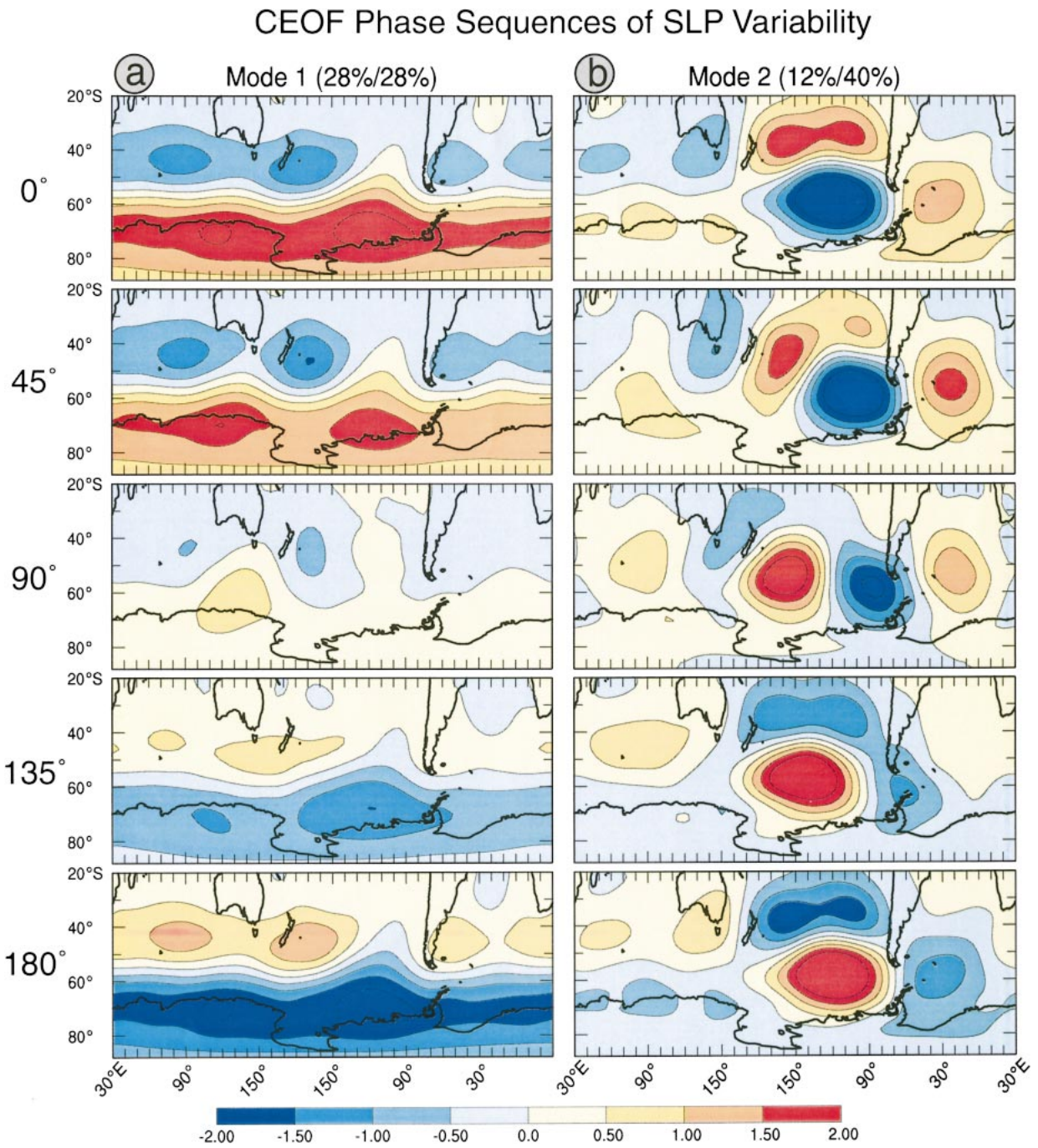

FIG. 1. Spatial phase sequences of the first two CEOF modes of area-weighted monthly SLP anomalies over the Southern Hemisphere from 20° to 90°S over the 20-yr record from 1982 to 2001. Each CEOF phase sequence extends over 180° of phase, representing the evolution of SLP variability over one-half cycles. (a) The first mode explains 28% of the monthly SLP variance and displays the evolution of the SAM over one-half cycle. (b) The second mode explains 12% of the monthly SLP variance and displays the evolution of the ACW over one-half cycle. Propagation is indicated in these phase sequences by following weights of like sign from one map to the next in the phase sequence. The color contours are given in units of standard deviation by the color bar at the bottom, with SLP weights normalized to yield unit variance over the phase sequence. See text for further details.

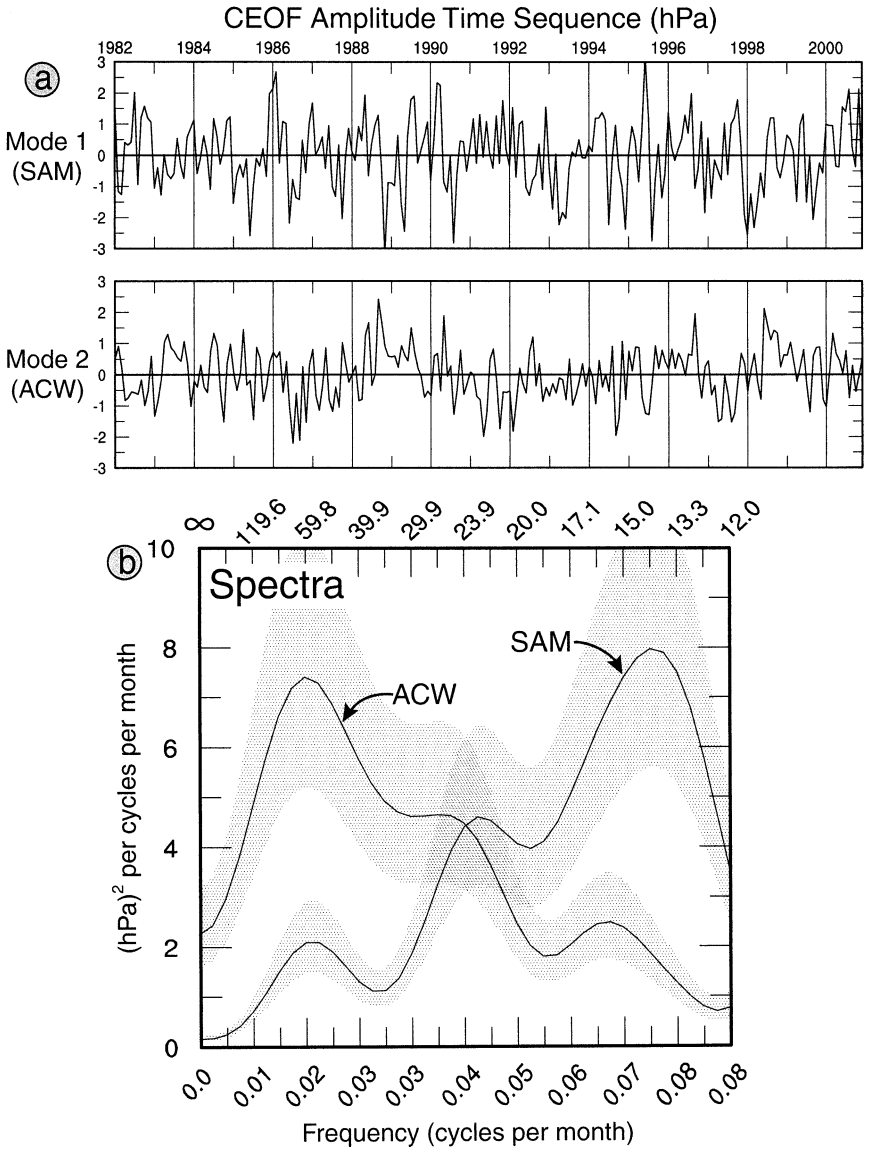

FIG. 2. (a) Time sequences of amplitude associated with the first and second CEOF modes of area-weighted monthly SLP anomalies extending over the 20 yr from 1982 to 2001. (b) These time sequences are accompanied by corresponding frequency power spectra in units of power spectral density [$(\text{hPa})^2$ per cycles per month], extending from the Nyquist period of 2 months to the longest period of 20 yr (Jenkins and Watts 1968). The error band of the dotted field yields the 95% confidence limits on each spectral density estimate.

propagating eastward across most of the Southern Ocean at a speed of ~90° of longitude per half cycle (i.e., ~45° of longitude per year). It has maximum amplitude in the Pacific sector of the Southern Ocean, nearly twice that in the Atlantic and Indian sectors. The path of the ACW in SLP variability can be seen following the subtropical front near 45°S in the eastern Atlantic, Indian, and western and central Pacific sectors of the Southern Ocean, then dipping to the south in the eastern Pacific and western Atlantic sectors to pass through Drake Passage near 60°S. This is consistent with the principal path of the ACW revealed by White and Chen (2002). On the other hand, the global spiral pattern of the ACW over the Southern Ocean observed in animation sequences of interanual SST and SLP anomalies (White et al. 1998) is missing in this CEOF phase sequence. As a result, the development of signal in the subtropical Pacific sector between 20°S and 45°S is no longer connected to that of the same sign along the sea ice edge near the Ross Sea. This is due to the interference of the wavenumber-2 component of the ACW with its wavenumber-3 component (Venegas 2003); the latter is suppressed when analyzing interannual SLP anomalies (White and Peterson 1996). The magnitude of SLP

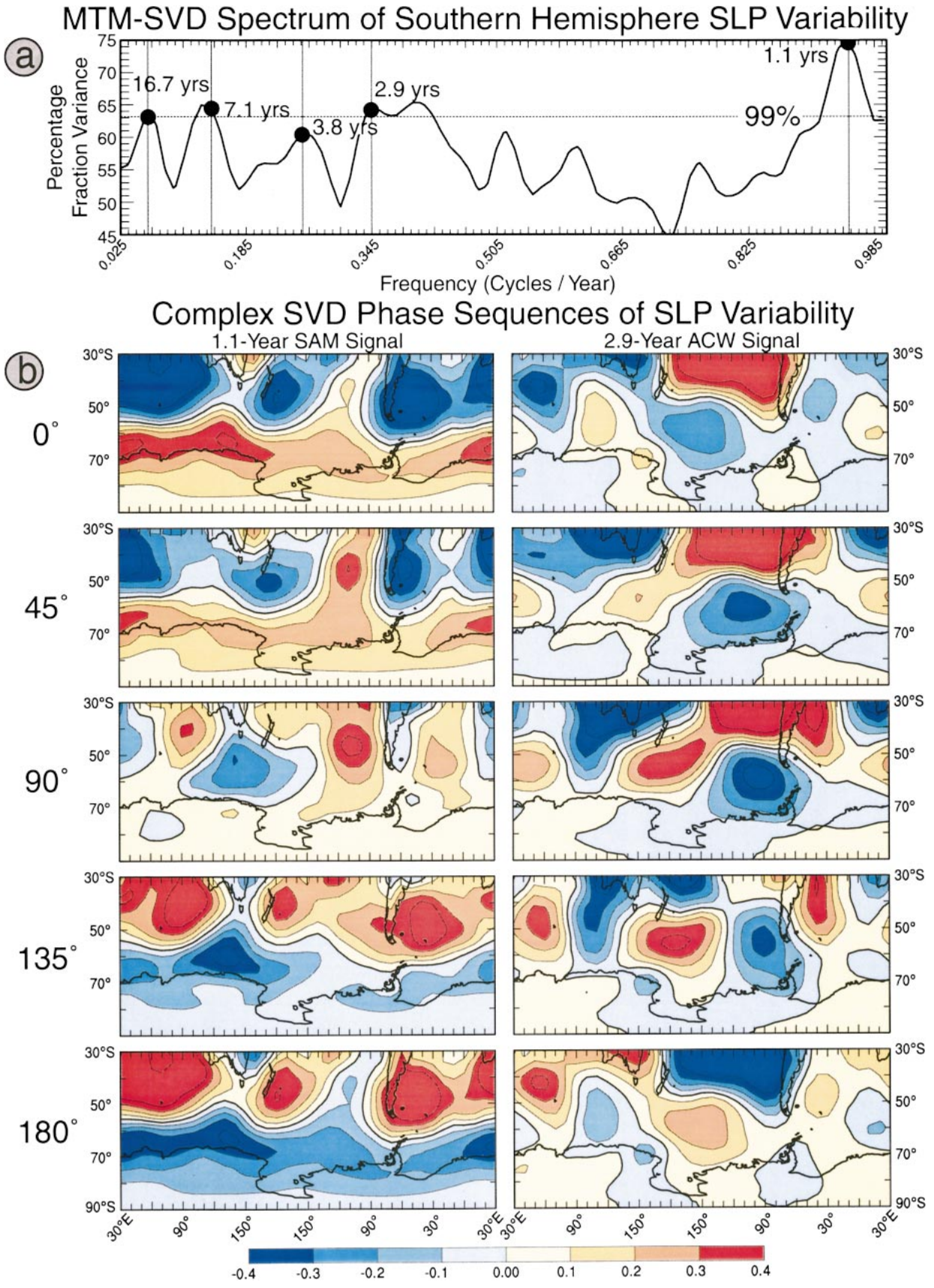

weights at 90° of phase are as large as those at 0° and 180° of phase, indicating that this CEOF mode is dominated by the propagating signal of the ACW, not the standing mode of the Pacific–South America (PSA) pattern, consistent with that observed by White et al. (2002). The relatively large amplitude of the ACW in the Pacific sector of the Southern Ocean occurs because it is forced by atmospheric teleconnections, stemming from the eastward phase propagation of the global ENSO wave (White and Cayan 2000) across the warm pool in the western Pacific Ocean (White et al. 2002).

On the face of it, these percentage of explained monthly SLP variance would appear to confirm the authors' statement concerning the dominance of the SAM over the ACW–ENSO in the Southern Ocean on interannual period scales. But, this applies only to monthly SLP variance, not to interannual SLP variance. To demonstrate this, we display the CEOF time sequences of amplitudes for each mode computed from the area-weighted SLP anomalies (Fig. 2a), together with their frequency spectra (Fig. 2b), overlapping the latter for better comparison. In computing these spectra, we detrended the CEOF time sequence of amplitudes in the normal course of prewhitening the data (Jenkins and Watts 1968). Here, we required the CEOF time sequences of amplitude to carry the monthly variance of each CEOF mode through a normalization of the CEOF phase sequences, which gives unit variance of the SLP weights therein (Fig. 1). The power spectra of the resulting amplitude time sequences (Fig. 2b) finds the SAM mode dominating the ACW mode for periods $<$ 1.5 yr. For periods of $\sim$2 yr, the SAM and ACW modes express similar spectral energy density. But, for periods of 3–7 yr the ACW mode dominates the SAM mode by one-half an order of magnitude or more. Over the entire frequency band, the power spectrum for the SAM mode is blue for periods longer than $\sim$1.2 yr, while that for the ACW–ENSO mode is red, peaking at a period near 5 yr. This latter peak was also observed in zonal wavenumber–frequency spectra computed from monthly SLP anomalies extending around the globe from 1982 to the present at constant latitudes of 56°S (White and Peterson 1996) and 50°S (White and Chen 2002). Thus, on interannual period scales of 3–7 yr, the CEOF mode representing the ACW and teleconnected ENSO signals dominated the CEOF mode, representing the SAM in its contribution to interannual SLP variability over the Southern Ocean over this record. The amplitude of the interannual ACW–ENSO mode [i.e., $(7.5 \times 0.02)^{1/2} =$ 0.39 hPa] is larger than that of the interannual SAM mode [i.e., $(2.0 \times 0.02)^{1/2} = 0.2$ hPa] by a factor of $\sim$2.

We confirm these results by applying MTM–SVD analysis of Mann and Park (1999) to the same SLP dataset, yielding the local fractional variance spectrum (Fig. 3a). This spectrum shows four signals that exceed the 99% confidence level, that is, near 1.1-, 2.9-, 7.1-, and 16.7-yr periods. The signals near 2.9-, 7.1-, and 16.7-yr periods are ACW in character, propagating eastward with global zonal wavenumber 2 or 3 (Venegas 2003), while the signal near the 1.1-yr period is SAM in character, mixed with zonal wavenumber-3 variability. To demonstrate this, we plot the phase sequences of the complex SVD modes for the signal near the 1.1-yr period and the signal near the 2.9-yr period (Fig. 3b). The former displays zonal uniform variability of the SAM at 0° and 180° phase, with low SLP weights all along the coast of Antarctic at 0° of phase, evolving toward high SLP weights at 180°, similar to the SAM CEOF mode (Fig. 1). On the other hand, the 2.9-yr signal (Fig. 3b) displays the global zonal wavenumber-2 and -3 variability and eastward propagation of the ACW. The phase sequence of the ACW signal near the 7.1-yr period (not shown) also propagates eastward with zonal global wavenumber 2. While the 1.1-yr period SAM and the 2.9-yr period ACW signals explain $\sim$75% and $\sim$65% of the local fractional variance in their frequency bands, respectively, the SAM contributes very little to the interannual variability. This is dominated by ACW variability of global zonal wavenumbers 2 and 3 (Venegas 2003).

Furthermore, Hall and Visbeck (2002) imply that the SAM dominates year-to-year variability in the winter sea ice pack forming around Antarctica each year. When CEOF analysis is applied to fall–winter–spring sea ice concentrations (SIC) around Antarctica over June–July–August–September–October (JJASO) for the 20 yr from 1982 to 2001 (National Snow and Ice Data Center 2002) (not shown), the ACW–ENSO mode is the dominant CEOF mode, as observed already by Gloersen and White (2001) and consistent with Yuan and Martinson (2000). It explains 35% of the year-to-year winter SIC variance over the 20-yr record. The SAM is found in the second CEOF mode, mixed with the global zonal wavenumber-3 pattern of variability, explaining 16% of the year-to-year winter SIC variance in the 20-yr record. These latter results are being prepared in a manuscript for submission to the *Journal of Geophysical Research*

←

FIG. 3. (a) Spectrum of the SLP local fractional variance as a function of frequency explained by the first MTM–SVD mode. The horizontal dashed line represents the 99% confidence limit in the spectrum. Signals occur at four spectral peaks >99% confidence level, that is, near the 1.1-, 2.9-, 7.1-, and 16.7-yr period. (b) Spatial phase sequences of the complex SVD modes for SLP variability in the SAM signal near the 1.1-yr period and the ACW signal near the 2.9-yr period. Five panels are chosen to represent $\sim$1/2 cycle of each signal extending over 180° of phase. Propagation is indicated in these phase sequences by following weights of like sign from one map to the next in the phase sequence. The SLP weights are color contoured, with blue (yellow to red) indicating negative (positive) weights, with the contours of the relative weights given in the color bar at bottom.

in collaboration with Ian Simmonds at the University of Melbourne and Per Gloersen at the Goddard Space Flight Center.

REFERENCES

Cai, W., and P. G. Baines, 2001: Forcing of the Antarctic circumpolar wave by El Niño–Southern Oscillation teleconnections. *J. Geophys. Res.*, **106,** 9019–9038.

Gloersen, P., and W. B. White, 2001: Reestablishing the circumpolar wave in sea ice around Antarctica from one winter to the next. *J. Geophys. Res.*, **106,** 4391–4395.

Hall, A., and M. Visbeck, 2002: Synchronous variability in the Southern Hemisphere atmosphere, sea ice, and ocean resulting from the annular mode. *J. Climate,* **15,** 3043–3057.

Jacobs, G. A., and J. L. Mitchell, 1996: Ocean circulation variations associated with the Antarctic circumpolar wave. *Geophys. Res. Lett.*, **23,** 2947–2950.

Jenkins, G. M., and D. G. Watts, 1968: *Spectral Analysis and Its Applications.* Holden-Day, 502 pp.

Kalnay, E., and Coauthors, 1996: The NCEP/NCAR 40-Year Reanalysis Project. *Bull. Amer. Meteor. Soc.,* **77,** 437–471.

Karoly, D. J., 1989: Southern Hemisphere circulation features associated with El Niño–Southern Oscillation events. *J. Climate,* **2,** 1239–1252.

Mann, M. E., and J. Park, 1999: Oscillatory spatio-temporal signal detection in climate studies: A multiple-taper spectral domain approach. *Advances in Geophysics,* Vol. 41, Academic Press, 1–31.

National Snow and Ice Data Center, 2002: Sea ice concentrations from Nimbus-7 SMMR and DMSP SSM/I passive microwave data 26 October 1978–31 December 2000. Vols. 1–3. NSIDC, ECD-ROMs, USA_NASA_0001-0003.

Preisendorfer, R. W., and C. D. Mobley, 1988: *Principal Component Analysis in Meteorology and Oceanography.* Elsevier, 425 pp.

Thompson, D., and M. Wallace, 2000: Annular modes in the extratropical circulation. Part I: Month-to-month variability. *J. Climate,* **13,** 1018–1036.

Venegas, S. A., 2003: The Antarctic circumpolar wave: A combination of two signals? *J. Climate,* **16,** 2509–2525.

White, W. B., and R. Peterson, 1996: An Antarctic circumpolar wave in surface pressure, wind, temperature, and sea ice extent. *Nature,* **380,** 699–702.

——, and D. R. Cayan, 2000: A global ENSO wave in surface temperature and pressure and its interdecadal modulation from 1900 to 1997. *J. Geophys. Res.*, **105,** 11 223–11 242.

——, and S.-C. Chen, 2002: Thermodynamic mechanisms responsible for the troposphere response to SST anomalies in the Antarctic circumpolar wave. *J. Climate,* **15,** 2577–2596.

——, ——, and R. Peterson, 1998: The Antarctic circumpolar wave: A beta effect in ocean–atmosphere coupling over the Southern Ocean. *J. Phys. Oceanogr.,* **28,** 2345–2361.

——, ——, R. J. Allan, and R. C. Stone, 2002: Positive feedbacks between the Antarctic circumpolar wave and the global El Niño-Southern Oscillation Wave. *J. Geophys. Res.*, **107**, 3165, doi:10.1029/2000JC000581.

Yuan, X., and D. G. Martinson, 2000: Antarctic sea ice extent variability and its global connectivity. *J. Climate,* **13,** 1697–1717.